Proceedings of the Institute of Acoustics

PASSIVE ACOUSTIC MONITORING OF SEABED GAS SEEPS - APPLICATION OF BEAMFORMING TECHNIQUES

J. Li	Institute of Sound and Vibration Research, University of Southampton, Southampton SO17 1BJ, U.K.
P. R. White	Institute of Sound and Vibration Research, University of Southampton, Southampton SO17 1BJ, U.K.
J. M. Bull	Ocean and Earth Science, University of Southampton, National Oceanography Centre, Southampton SO14 3ZH, U.K.
T. G. Leighton	Institute of Sound and Vibration Research, University of Southampton, Southampton SO17 1BJ, U.K.
B. Roche	Ocean and Earth Science, University of Southampton, National Oceanography Centre, Southampton SO14 3ZH, U.K.
J. W. Davis	Ocean and Earth Science, University of Southampton, National Oceanography Centre, Southampton SO14 3ZH, U.K.

INTRODUCTION

THE INCREASE OF GREENHOUSE GAS IN THE ATMOSPHERE HAS RESULTED IN GLOBAL WARMING AND THE CONSEQUENT CHANGE IN THE CLIMATE, WHICH POSES THREAT TO THE HABITABILITY OF THE PLANET. TO MITIGATE THE IMPACT OF ANTHROPOGENIC GREENHOUSE GAS EMISSION, MARINE CARBON DIOXIDE CAPTURE AND STORAGE (CCS) HAS BEEN IDENTIFIED AS AN IMPORTANT STRATEGY, WHICH AIMS TO PERMANENTLY LOCK CO_2 IN SUB-SEABED GEOLOGICAL RESERVOIRS.[1] THE RISK MANAGEMENT OF THE MARINE CCS STRATEGIES REQUIRES MONITORING OF THE STORAGE SITE TO ENSURE ITS INTEGRITY.[2,3] CONSEQUENTLY, EFFECTIVE MONITORING TECHNIQUES ARE URGENTLY REQUIRED. RECENT TECHNOLOGY DEVELOPMENTS FOR SUCH MONITORING INCLUDE INNOVATIVE METHODS IN TERMS OF ACOUSTICS, OPTICS, CHEMISTRY, AND BIOLOGY.[4-6]

BEAMFORMING IS A FUNDAMENTAL SIGNAL PROCESSING METHOD BY WHICH DATA FROM AN ARRAY OF SENSORS IS COMBINED TO CREATE A SYSTEM WITH A DIRECTIONAL RESPONSE. IT ACHIEVES SPATIAL SELECTIVITY BY COMBINING ELEMENTS IN A SENSOR ARRAY IN SUCH A WAY THAT SIGNALS AT PARTICULAR ANGLES EXPERIENCE CONSTRUCTIVE INTERFERENCE WHILE OTHERS EXPERIENCE DESTRUCTIVE INTERFERENCE.[7] A FAMILIAR TECHNIQUE WHICH FACILITATES THE ENHANCEMENT OF A SIGNAL ALONGSIDE LOCALIZATION IS THE MINIMUM VARIANCE DISTORTIONLESS RESPONSE (MVDR) BEAMFORMER.[7] THE MVDR BEAMFORMER ADJUSTS ITS RESPONSE TO MINIMIZE CONTAMINATION FROM SURROUNDING NOISE SOURCES, SO POTENTIALLY OFFERS GREAT IMPROVEMENTS IN SIGNAL-TO-NOISE RATIO (SNR) AND HIGH RESOLUTION.[7]

TO DEMONSTRATE THE EFFECTIVENESS OF ARRAY PROCESSING FOR PASSIVE MONITORING OF GAS SEEPS, IN THIS PAPER, WE PROPOSE AND INVESTIGATE A BUBBLE FOCUSED BEAMFORMING METHOD AS A PASSIVE ACOUSTIC TECHNIQUE APPLIED ON THE UNDERSEA GAS SEEPS LOCALIZATION. THE PROPOSED BEAMFORMING PROCESSES BROADBAND BUBBLE SOUND DATA BASED ON THE MVDR ALGORITHM. TO TEST THE EFFECTIVENESS OF THE PROPOSED BEAMFORMING, WE CONDUCTED A CONTROLLED GAS RELEASE EXPERIMENT IN THE CENTRAL NORTH SEA ASSOCIATED WITH THE PROJECT STEMM-CCS (STRATEGIES FOR ENVIRONMENTAL MONITORING OF MARINE CARBON

CAPTURE AND STORAGE HTTP://WWW.STEMM-CCS.EU/). IN THE EXPERIMENT, A HYDROPHONE ARRAY COMPRISING FIVE HYDROPHONES WAS DEPLOYED IN A WATER DEPTH OF 120 M ON THE SEAFLOOR TO COLLECT THE SOUND DATA ASSOCIATED WITH THE GAS BUBBLE RELEASE.

EXPERIMENT

The STEMM-CCS controlled gas release experiment was completed between 500 and 1000 m southeast of the Goldeneye platform,[8] around 100 km east of Scotland. Directional drilling took place to insert a curved pipe, tipped with a gas diffuser, so that the pipe end was 4 m beneath the seafloor in a water depth of 120 m. CO2 gas was injected into the overlying unconsolidated sediments, over a 5-week period, during which the flow rate was increased from 0 to 143 kg/day (50 L/min at standard temperature (T) and pressure (P) (STP) condition).[9, 10] Note that the higher pressure at the *in situ* site (120 m beneath the sea surface) makes the gas flow rate [13] times lower than that at the STP condition. The temporal and spatial behavior of gas seeps generated at the sea floor due to the injection were monitored using the hydrophone array close to the gas injection site.

At the highest release rate, 143 kg/day, eight seeps with moderate and relatively high flow rates[9] were optically observed by underwater cameras and acoustically recorded (Figure 1). The hydrophone wall (Figure 2(a)) was positioned 3.3 m east of the point which is directly above the gas diffuser (Figure 1). Five hydrophones (Geospectrum M36, GTI) were linked to the acoustic recorder (RS-ORCA Multi-Channel Passive Acoustic Recorder, RS Aqua). These hydrophones were absolutely calibrated for this water depth and temperature with receive sensitivity of -164.5 dB re: 1 V/µPa. Each of the channels was sampled at 96 kHz, after a gain of 15 dB was applied. Figure 2(b) shows bubbles were emitting from the seafloor.

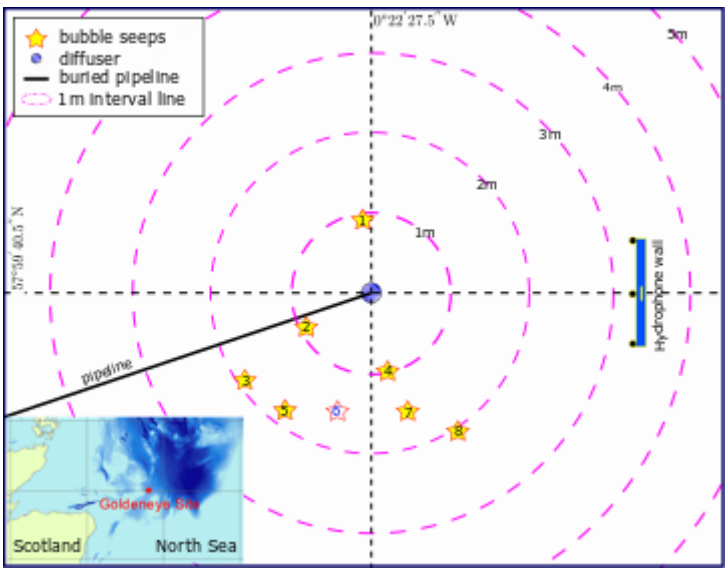

Figure 1: Mapped gas seep locations when the CO2 release rate was 143 kg/day. Beneath the central dot is the gas diffuser; stars represent eight observed gas seeps. The hydrophone wall was placed at 3.3 m east from the central point. Concentric dashed circles (magenta) show distances from experiment epicenter in meters. The inset map shows the location of the experiment in the North Sea.

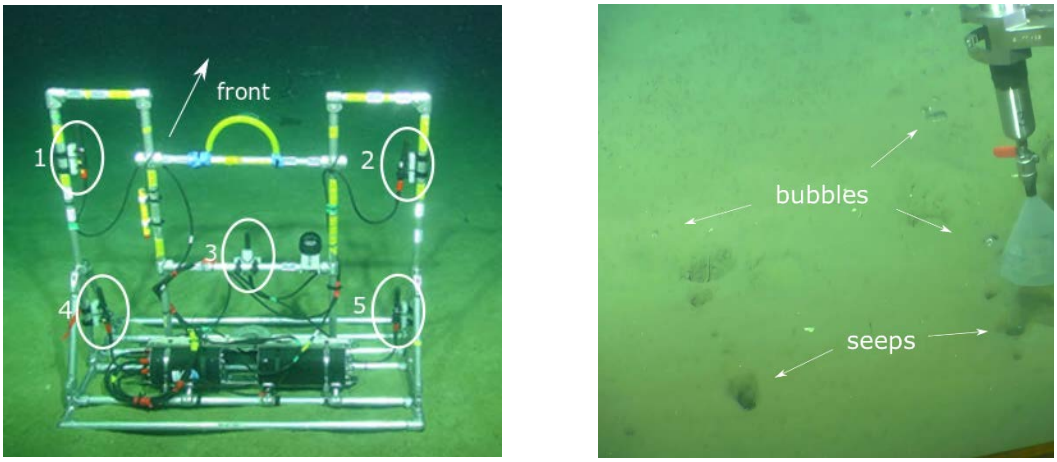

(a) Hydrophone wall ***(b) Seeping bubbles***

Figure 2: Photographs showing (a) the hydrophone wall (HW) positioned on the seafloor, in front of which is the seep region; (b) CO2 gas bubbles emitting from the gas seeps originated from the sub-seabed.

BUBBLE FOCUSED BROADBAND MVDR BEAMFORMING TECHNIQUE

Underwater ambient noise generally has a significantly wider bandwidth than the sound of an individual bubble. At low SNRs, the target signal was too weak to be identified without appropriate analysis. To improve the probability of success with beamforming, the signature of the target signal source needs to be firstly considered in an identification process. To identify single bubbles for beamforming, we apply the single bubble identification method detailed in Li et al.[10] on the received acoustic signals. To remove detections which are not similar to bubbles, the method identifies sounds above thresholds by using typical time duration and frequency bandwidth of a single bubble acoustic waveform. By processing the spectrogram of beamformed acoustic signals with thresholds, a series of bubble acoustic pulses are identified with each pulse involving a patch of frequencies forming a bandwidth of $[f_{\text{start}}, f_{\text{end}}]$. The signal is then band-pass filtered over the band $[f_{\text{start}}, f_{\text{end}}]$ corresponding to the acoustic bandwidth of a bubble and a 15 ms window applied around the detected event, creating what we term a bubble data package.

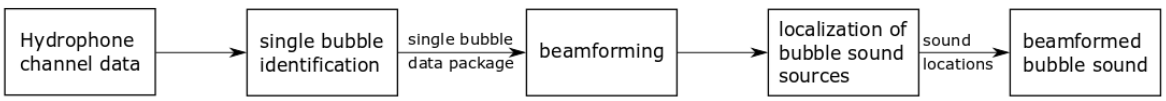

Figure 3: The approach of localizing bubble sound sources and generating beamformed bubble signals.

The stages of the bubble sound source localization method are shown in Figure 3. The data packages from all the hydrophones are used as the basis for the localization procedure. There were eight seeps distributed at different ranges and we do not know the relative ebullition at each seep. In the gas seep region all eight seeps are observed west of the hydrophone walls, with each ebullition site producing bubble sounds. To localize these identified bubble sounds sources, we apply a bubble focused broadband MVDR beamformer. As an adaptive beamforming, the MVDR beamformer mitigates the effect of the noise by minimizing the overall output power whilst maintaining unit gain in the direction of the source.[7]

Consider N gas seeps radiating bubble sound received by M omni-directional hydrophones, in which each hydrophone output is an attenuated and delayed version of the data package with bubble sound. In a short period starting from the instant at which a bubble pulsates, the bubble damping leads to the variation of its resonance frequency revealing a frequency bandwidth of the radiated sound. To consider such a bubble signal in a broadband, we divide the frequency band $[f_{\text{start}}, f_{\text{end}}]$ for a single bubble into a number of frequency bins f_i, where $i = 1, \dots, I$ and I is the number of bins.

The location estimator computes the spatial power distribution of the received signal by processing the hydrophone signals. A well-known rule of thumb is that $K \geq 2M$ independent and identically distributed snapshots are required to obtain a well-conditioned cross spectral density matrix (CSDM) estimate.[12] In this paper, we apply $K = 16$, i.e. for a 15 ms bubble data package, the length of each snapshot is about 1 ms. For each frequency bin fi, the weight factor of the bubble focused broadband MVDR beamforming is based on the computation of an M x M CSDM $Q(f_i)$:[13]

$$\mathrm{Q}(f_i) = \frac{1}{K}\sum_{k=1}^{K} X_k(f_i){X_k}^H(f_i) + \kappa I_N, \tag{1}$$

where $X_k(f_i) = [X_{1,k}(f_i); \dots; X_{M,k}(f_i)]$ is the Fourier transformed frequency domain hydrophone channel data at the frequency bin fi and the kth snapshot, I_M is an M x M identity matrix, and κ is a regularization factor which is a small positive number used to improve the condition of the matrix.

The matrix $Q(f_i)$ is used for obtaining the spatial power at every gas seep grid location using the MVDR algorithm.[7] For a frequency bin f_i, the steering vector at the n^{th} seep is given by:[11]

$$v_{mn}(f_i) = [1, \dots, a_{mn}e^{j2\pi f_i \tau_{mn}}, \dots, a_{mNn}e^{j2\pi f_i \tau_{mN}}]^T, \tag{2}$$

where $[]^T$ denotes the transpose of a matrix, and $a_{mn} = \frac{d_{\text{ref},n}}{d_{mn}}$ is the attenuation factor, where d_{mn} and $d_{\text{ref},n}$ denote the three-dimensional Euclidian distances between the n^{th} seep and the m^{th} sensor and the reference sensor, respectively. Herein, as implied by the form of (2), the reference sensor is taken to be hydrophone 1. $\tau_{mn} = \frac{d_{mn} - d_{\text{ref},n}}{c}$ is the delay, where c is the underwater sound speed assumed to be constant and measured in the experiment to be 1484 m/s. The sound power at frequency f_i from the n^{th} gas seep:

$$P_n(f_i) = [{v_n}^H(f_i)Q^{-1}(f_i)v_n(f_i)]^{-1}. \tag{3}$$

The total power for all frequencies of interest is computed by summing powers across frequency:

$$P_n = \sum_{f_i = f_{start}}^{f_{end}} P_n(f_i). \tag{4}$$

The point with the highest power is considered to correspond to the location of the bubble sound source. To situate this specific experiment with a central gas release point, a circular grid with an angular increment of $\theta = 5^\circ$ and a range step of 0.25 m from the central point of the experimental area is used (see Figure 1).

For an identified bubble source location n, to reduce interference from other directions, the optimal beamformer weight vector $W_n(f_i)$ is given by:[7]

$$w_n(f_i) = Q^{-1}(f_i)v_n(f_i)P_n(f_i). \tag{5}$$

Then the frequency domain beamformed signal is:

$$Y_n(f_i) = W_n^H(f_i)X(f_i). \tag{6}$$

EXPERIMENTAL RESULTS

In this section, with the data collected in the STEMM-CCS experiment, we select data package containing single bubble sounds based on a single bubble identification algorithm,[10] to verify the localization performance using the bubble focused broadband beamforming technique.

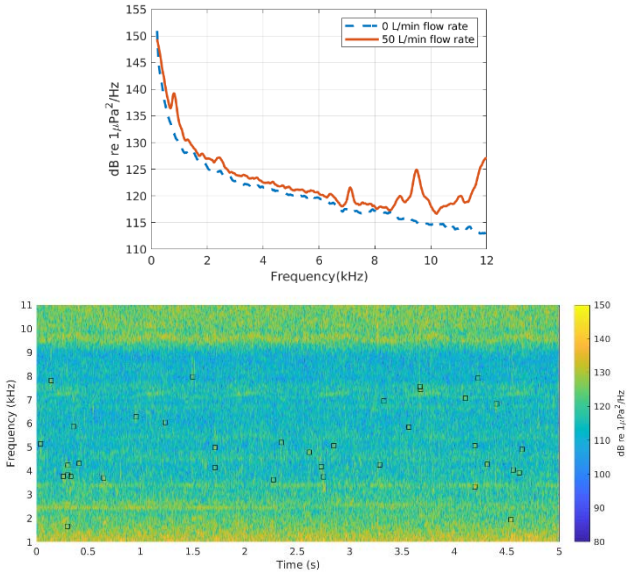

(a) Power spectral density ***(b) Spectrogram***

Figure 4: Power spectral density (PSD) and spectrogram of signals measured on a single hydrophone (No. 3). (a) PSD comparison of the sound received at gas injection rates 143 kg/day and 0 kg/day. Peaks at 1, 2.5, 7, 8.5 and 12 kHz are identified as ship or underwater vehicular noise. (b) Spectrogram of 5 s sound. Single bubbles are identified and marked using squares, predominantly in the band 2 to 8 kHz.

Figure 4(a) shows the average power spectral density (PSD) of the data collected on 20th May 2019. To compare the PSD with and without gas injection, it is worth building background noise baseline before the experiment at the same site, shown as dashed line in the figure recorded on 9th May 2019 prior to the gas release experiment. The spectral peaks at 1, 2.5, 7, 8.5 and 12 kHz seen in the 143 kg/day data in Figure 4(a) were identified as ship noise or underwater vehicular noise. Apart from these peaks, there is not much difference between the cases of gas injection rate 143 kg/day and 0 kg/day (background noise).

SINGLE BUBBLE SELECTION

Figure 4(b) shows the spectrogram of 5 s data as an example of data measured by a single hydrophone (No. 3) during the experiment at the gas injection rate 143 kg/day. Using a single bubble identification algorithm,[10] we identify single bubble formation events through their temporal and spectral characteristics, i.e. the pulsation length, frequency bandwidth, and amplitude. These identified events are marked using squares , from which we can see that the majority number of

bubbles are located in the frequency interval between 2 kHz and 8 kHz, corresponding to bubble radius about 5 mm to 1 mm at this depth.

BEAMFORMING RESULTS

From the selection, we obtain a sequence of bubble data packages. For each data package, we apply the beamforming algorithm presented in Section 3. We take every bubble, which has a resonance frequency f, to compute the power at f for every location. Figure 5 shows examples of localisation results of four bubble data packages at resonance frequencies close to 2 kHz to 8 kHz. Note that the closest resonance frequency f here denotes an interval of $[f - 0.5, f + 0.5]$ kHz, e.g. 2 kHz denotes an interval $[1.5, 2.5]$ kHz.

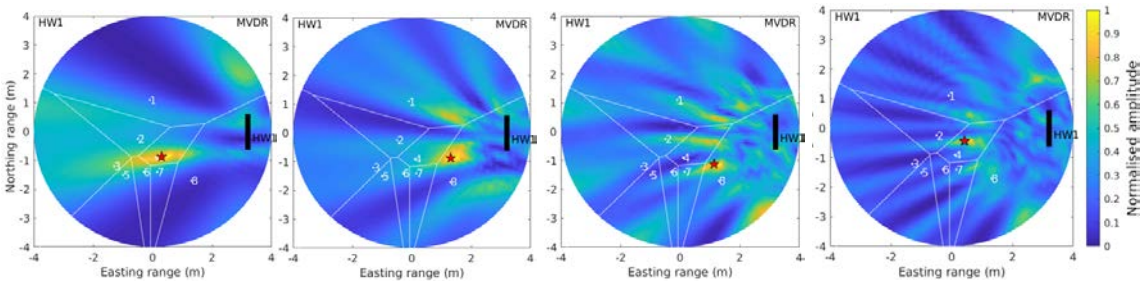

(a) 2 kHz ***(b) 4 kHz*** ***(c) 6 kHz*** ***(d) 8 kHz***

Figure 5: MVDR beamforming for the localization of single bubbles at frequencies. (a) 2 kHz; (b) 4 kHz; (c) 6 kHz; (d) 8 kHz. Red stars are localized bubble sound sources with the highest power amplitude.

Since there were eight significant seeps at different locations within the experimental area, one of our goals is to try to associate each bubble sound with a specific seep location. Voronoi diagram[14] is added to each of the localization map, showing boundary around a seep that includes all points closer to it than to any other seep. From Figure 5 we can see that the MVDR beamforming provides reasonable localization results.

SNR (SIGNAL-TO-NOISE) IMPROVEMENT

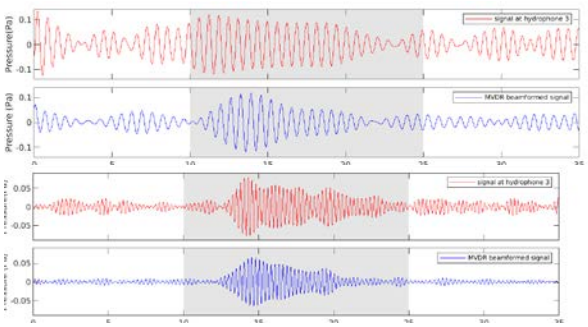

(a) 2 kHz ***(b) 4 kHz***

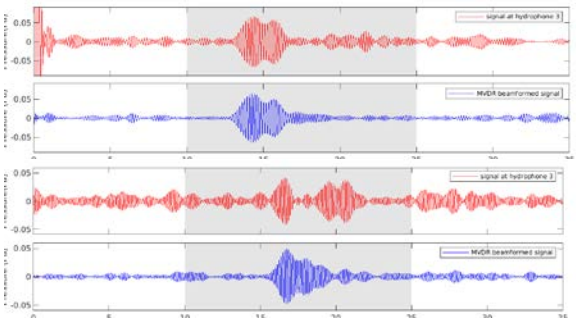

(c) 6 kHz ***(d) 8 kHz***

Figure 6: Comparison of acoustic signal waveforms received at hydrophone 3 (red) and beamformed signals (blue) at various frequencies: (a) 2 kHz; (b) 4 kHz; (c) 6 kHz; (d) 8 kHz. In all these cases, the bubble SNR has been improved, with typical bubble signatures more visible inside the grey scale.

Figure 6 shows comparisons of the data package waveforms received at hydrophone 3 (red) and the MVDR beamformed data package waveforms (blue) at various frequencies from 2 kHz to 8 kHz. In all the cases, the bubble signatures from the beamformed signals are more visible compared to that received directly by hydrophone channels, which reveals an improvement of the bubble SNR. The bubble pulsation length is typically 15 ms and can be dominant in 5 ms, and the measured pressure amplitude for each bubble acoustic data package (grey scale) is from 0.05 Pa to 0.1 Pa in all the four cases.

To statically show the bubble SNR improvement by using beamforming, we select a signal segment with 1500 bubbles identified. Figure 7 shows that the SNR of the data package is improved by an average of 3 dB using beamforming across the frequency band [2, 10] kHz. The dominant resonance frequency of gas bubbles are from 5 kHz to 8 kHz, showing the highest SNR improvement up to 5 dB.

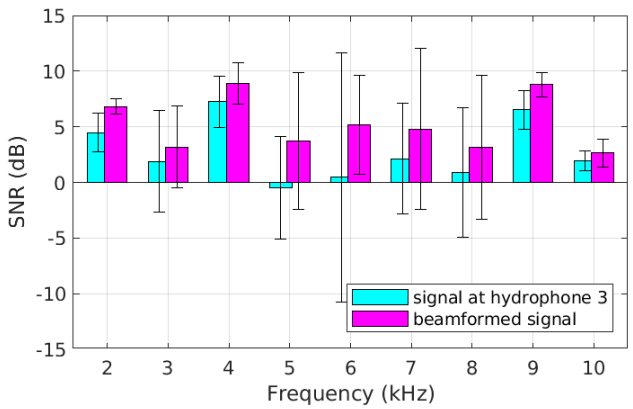

Figure 7: MVDR beamforming for the localization of single bubbles at frequencies. (a) 2 kHz; (b) 4 kHz; (c) 6 kHz; (d) 8 kHz. Red stars are localized bubble sound sources with the highest power amplitude.

CONCLUSION

In this work, we presented a bubble focused MVDR beamforming for the localization of CO_2 gas seeps, and demonstrated that array processing can enhance the SNR of seep sounds and can

localize bubble sounds with the acoustic data collected in the STEMM-CCS experiment in the central North Sea. Bubble SNR has been improved using the MVDR beamforming technique at various frequencies between 2 and 8 kHz. Due to the sound wave interference in the acoustic propagation channel, the estimated locations of bubble sound sources are somewhat closer to the hydrophone array than that from the observed gas seep locations.

ACKNOWLEDGEMENTS

Funding was provided by the European Unions Horizon 2020 research and innovation programme under the grant agreement number 654462 (STEMM-CCS). We are grateful to the Captain of the RRS 'James Cook' and crew for enabling the scientific measurements at sea during the JC180 cruise.

REFERENCES

1. J. Blackford, H. Stahl, J. M. Bull, B. J. Bergès, M. Cevatoglu, A. Lichtschlag, D. Connelly, R. H. James, J. Kita, D. Long, et al., Detection and impacts of leakage from sub-seafloor deep geological carbon dioxide storage, Nature climate change 4 (11) (2014) 1011. doi:10.1038/nclimate2381.
2. T. G. Leighton, P. R. White, Quantification of undersea gas leaks from carbon capture and storage facilities, from pipelines and from methane seeps, by their acoustic emissions, Proceedings of the Royal Society A: Mathematical, Physical and Engineering Sciences 468 (2138) (2011) 485–510. doi:10.1098/rspa.2011.0221.
3. J. Blackford, J. M. Bull, M. Cevatoglu, D. Connelly, C. Hauton, R. H. James, A. Lichtschlag, H. Stahl, S. Widdicombe, I. C. Wright, Marine baseline and monitoring strategies for carbon dioxide capture and storage (CCS), International Journal of Greenhouse Gas Control 38 (2015) 221–229. doi:10.1016/j.ijggc.2014.10.004.
4. J. Li, B. Roche, J. M. Bull, P. R. White, J.W. Davis, M. Deponte, E. Gordini, D. Cotterle, Passive acoustic monitoring of a natural CO2 seep site - implications for Carbon Capture and Storage, International Journal of Greenhouse Gas Control 93 (1) (2020) 102899 – 102910. doi:10.1016/j.ijggc.2019.102899.
5. K. Shitashima, Y. Maeda, A. Sakamoto, Detection and monitoring of leaked CO2 through sediment, water column and atmosphere in a sub-seabed CCS experiment, International Journal of Greenhouse Gas Control 38 (2015) 135–142. doi:10.1016/j.ijggc.2014.12.011.
6. J. J. Roberts, S. M. Gilfillan, L. Stalker, M. Naylor, Geochemical tracers for monitoring offshore CO2 stores, International Journal of Greenhouse Gas Control 65 (2017) 218–234. doi:10.1016/j.ijggc.2017.07.021.
7. J. Capon, High-resolution frequency-wavenumber spectrum analysis, Proceedings of the IEEE 57 (8) (1969) 1408–1418. doi:10.1109/PROC.1969.7278.
8. Shell, Goldeneye Gas Platform, United Kingdom. (2017). URL http://www.offshore-technology.com/projects/goldeneye/
9. A. Flohr, J. Matter, R. James, A. Lichtschlag, K. Peel, C. Pearce, D. Connelly, Quantification of leakage from sub-seabed CO2 storage using natural and added geochemical tracers, International Journal of Greenhouse Gas Control 105 (2020) 103244-103255. doi: 10.1016/j.ijggc.2020.103244.
10. J. Li, P. R. White, B. Roche, J. M. Bull, T. G. Leighton, J. W. Davis, J. W. Fone, Acoustic and optical determination of bubble size distributions - quantification of undersea gas emissions, International Journal of Greenhouse Gas Control (2020) to be presented.
11. J. Bitzer, K. U. Simmer, Superdirective microphone arrays, in: Microphone arrays, Springer, 2001, pp.19–38.

12. J. Capon, N. Goodman, Probability distributions for estimators of the frequency-wavenumber spectrum, Proceedings of the IEEE 58 (10) (1970) 1785–1786. doi:10.1109/PROC.1970.8014.
13. S. Haykin, J. H. Justice, N. L. Owsley, J. L. Yen, A. C. Kak, Array signal processing, Prentice-Hall, Inc., Englewood Cliffs, NJ, 1985.
14. C. K. Yap, AnO (n logn) algorithm for the voronoi diagram of a set of simple curve segments, Discrete & Computational Geometry 2 (4) (1987) 365–393. doi:10.1007/BF02187890.